Pergamon

Cement and Concrete Research 32 (2002) 565–576

CEMENT AND CONCRETE RESEARCH

Effects of the incorporation of Municipal Solid Waste Incineration fly ash in cement pastes and mortars II: Modeling

S. Rémond[a,b,*], D.P. Bentz[c], P. Pimienta[a]

[a]CSTB, 84 avenue Jean Jaurès, Champs sur Marne, 77421 Marne la Vallée cedex 2, France
[b]LMT ENS de Cachan, 61 avenue du Président Wilson, 94235 Cachan Cedex, France
[c]BFRL NIST, 100 Bureau Drive Stop 8621, Gaithersburg, MD 20899-8621, USA

Received 9 November 2000; accepted 29 October 2001

Abstract

This work falls within the scope of the general problem of the assessment of concretes manufactured from waste materials. The main objective is to study the long-term evolution of these materials during leaching using the cellular automata-based hydration model developed at the National Institute of Standards and Technology (NIST). The work is based on the analysis of mortars and cement pastes containing experimental waste: Municipal Solid Waste Incineration fly ash (MSWI fly ash). After having determined the mineralogical composition of the MSWI fly ash and its interactions with cement during hydration, presented previously as Part I, the phases comprising the fly ash have been incorporated into the hydration model. The increase in porosity of cement pastes containing MSWI fly ash during leaching has then been simulated. Finally, a simplified leaching model has been developed to study the influence of the changes in microstructure on the release of calcium and sodium.

Keywords: Hydration; Leaching; Microstructure; Diffusion; Transport properties

1. Introduction

This study contributes to the development of a methodology for assessing concretes manufactured from waste materials. The methodology is based on the study of mortars containing an experimental waste: Municipal Solid Waste Incineration fly ash (MSWI fly ash) [1,2].

The microstructure of concretes containing waste materials is likely to change considerably as the material ages due to the effects of carbonation, leaching, etc. These changes can affect the kinetics of penetration of aggressive agents inside the material and the kinetics of release of chemicals into the environment. The study of the microstructural evolution of concrete containing waste is therefore very important in order to predict its long-term behavior.

To study the long-term evolution of the microstructure of concretes containing waste during the leaching process, the CEMHYD3D hydration model developed at the National Institute of Standards and Technology (NIST) by Bentz and Garboczi [3] has been applied to cement pastes containing MSWI fly ash. The experimental study carried out to determine the input data needed for model execution has been presented in the first part of this article [4]. In this second part, assumptions of the model and the results obtained are presented.

The experimental study [4] has sufficiently characterized the MSWI fly ash so that it can be incorporated into the hydration model. The hydration of cement pastes in the presence of MSWI fly ash has then been simulated. The influence of MSWI fly ash on the quantity of hydrates formed and on the capillary porosity and its connectivity has in particular been studied. The evolution of the diffusion coefficient of pure cement pastes and cement pastes containing MSWI fly ash during leaching has been simulated. Finally, a macroscopic leaching model has been developed to assess the effects of the changes in transport properties of cement pastes containing fly ash on the kinetics of the release of chemicals into the environment.

* Corresponding author. IUP GCI, S MailGay-Lussac, Neuville Sur Oise, Cergy-Pontoise Cedex, 95031, France.
E-mail address: sebastien.remond@iupgc.u-cergy.fr (S. Rémond).

0008-8846/02/$ – see front matter
PII: S0008-8846(01)00722-0

2. Incorporation of MSWI fly ash in the hydration model

2.1. Modeling MSWI fly ash

2.1.1. Shape and size of the particles

In the CEMHYD3D hydration model, solid grains (cement, fly ash, fillers, etc.) are represented by digitized spherical particles whose diameter is an odd integer number of pixels. This representation allows one to easily locate each grain, knowing its radius and the position of its central pixel. In the model, MSWI fly ash particles are similarly represented by digitized spherical particles.

The scale chosen for the model is 1 μm/pixel. This provides a satisfactory representation of the microstructure of cement pastes [5]. Cubic pixels (1 μm) allow one to represent the size of the capillary pores and of the cement, fly ash and filler particles. The calculation volume used in the model is a cube 100 pixels on a side (i.e. 100 μm). The maximum radius of the particles has been limited to one-fifth of the side of the calculation volume so that the maximum diameter of the particles is 41 pixels for a $100 \times 100 \times 100$ pixel microstructure.

However, laser granulometric analysis of the MSWI fly ash has shown that the greatest part of the particles have sizes between 50 and 500 μm (the finest grains are smaller than 1 μm). The granulometry of the ash introduced into the model (diameter limited to a maximum of 41 μm) is therefore quite different from the experimental granulometry. The difference between experimental granulometry and granulometry of the digitized particles in the model is much smaller for the cement grains (as 82% of the grains are smaller than 41 μm).

2.1.2. Mineralogical composition of the MSWI fly ash

X-ray diffraction (XRD) analysis and X-ray spectrometric analysis performed on the MSWI fly ash have allowed determination of an approximate mineralogical composition of the material (see Part I of the article [4]). Six phases have been identified: AS,[1] CAS_2, chlorides, $CaSO_4$ (*CS*), quartz and an inert phase. For modeling hydration, the quartz in the MSWI fly ash was considered as an inert material, since well-crystallized silica is poorly reactive in cement pastes.

XRD analysis revealed the presence of halite (NaCl) and sylvite (KCl) in the MSWI fly ash, whereas chlorides have been identified as calcium chloride with X-ray spectrometric analysis. As was observed in the first part, the presence of NaCl and KCl in fly ash coming from a MSWI plant operating with a wet scrubber is more probable than that of $CaCl_2$. However, considering chlorides as $CaCl_2$ simplifies the model. Indeed, alkali ions such as Na^+ and K^+ are not currently taken into account in the hydration model (however, alkali ions can modify the solubility of some hydrates such as ettringite or Friedel's salt). Therefore, for the modeling, we consider that chlorides are present as $CaCl_2$. Table 1 shows the volume fractions of the six mineral phases of the MSWI fly ash used in the model.

Table 1
Volume fractions of the six mineral phases identified by X-ray spectrometric analysis in the MSWI fly ash (%)

Mineral phases	CAS_2	AS	$CaCl_2$	$CaSO_4$	Quartz	Inert
Volume fraction (%)	48.2	10.5	21.0	3.9	7.6	8.8

Observations by scanning electron microscopy (SEM) and X-ray spectrometric analysis have shown that, although the mineralogical composition of MSWI fly ash is quite heterogeneous, the composition of individual particles is rather homogeneous (one or two phases). We have therefore decided to randomly distribute the mineral phases amongst the fly ash particles so that each particle is made of only one single phase. However, chlorides have not been incorporated in the model as solid particles. Indeed, representing the initial mix as a suspension of solid grains in water implies that the hydration of those grains begins once all of the particles have reached their final positions. Between the beginning of mixing (first contact between water and cement) and the moment when particles occupy their final position (after vibration), several hours can pass. So, the representation of the initial mix as fixed spherical particles implies that the chemical reactions occurring between the beginning of mixing and the end of the vibration are negligible in comparison to those occurring after the vibration of the concrete. This assumption is certainly not realistic for the dissolution of the chlorides present in the MSWI fly ash. Indeed, a wash test of MSWI fly ash in demineralized water for 3 min has shown that the extraction of chlorides was almost complete [6]. So, the dissolution of chlorides is certainly complete long before the particles of the mix reach their final position. Chlorides have therefore been incorporated into the model directly within the interstitial solution from the beginning of the hydration; they have not been included as solid particles.

2.2. Formation of hydration products

XRD analysis performed on cement pastes containing MSWI fly ash has revealed the formation of Friedel's salt ($C_3A(CaCl_2)H_{10}$) due to the presence of the fly ash. This hydrate is formed from the reactions between the chlorides of the MSWI fly ash and the aluminates and aluminoferrites of the cement. The following reactions have been included in order to simulate the formation of Friedel's salt (the volume stoichiometric coefficients are indicated below each compound) [7]:

$$\underset{1.7261}{C_3A} + \underset{1}{CaCl_2} + \underset{3.487}{10H} \rightarrow \underset{5.747}{C_3A(CaCl_2)H_{10}}$$

$$\underset{2.4797}{C_4AF} + \underset{1}{CaCl_2} + \underset{4.882}{14H} \rightarrow \underset{5.747}{C_3A(CaCl_2)H_{10}} + \underset{0.641}{CH} + \underset{1.3522}{FH_3}$$

[1] Conventional cement chemistry notation is used throughout this article: C = CaO, S = SiO_2, A = Al_2O_3, F = Fe_2O_3, H = H_2O, and *S* = SO_3.

XRD analysis has also revealed that the quantity of ettringite formed in cement pastes containing MSWI fly ash is greater than that formed in pure cement pastes. The sulfates of MSWI fly ash can indeed react with the aluminates and the aluminoferrites to form ettringite and monosulfoaluminate. The formation of ettringite has already been taken into account in the hydration model [5]. It can be formed from the reaction between C_3A and C_4AF and the gypsum of the cement. To take into account the formation of ettringite from the anhydrite in the MSWI fly ash, a reaction for the conversion of anhydrite to gypsum has been added to the model. Gypsum formed from anhydrite can then react with the aluminates and aluminoferrites to form ettringite. The reaction for the conversion of anhydrite into gypsum is the following [7]:

$$\underset{1}{C\underline{S}} + \underset{0.69}{2H} \rightarrow \underset{1.423}{C\underline{S}H_2}$$

Kessler et al. [8] have identified the formation of pozzolanic reaction products, in particular stratlingite (C_2ASH_8), in cement pastes containing MSWI fly ash. This hydrate has not been identified in our experiments. However, to take into account the pozzolanic properties of the MSWI fly ash, the formation of stratlingite from the aluminosilicate (AS) and the calcium aluminodisilicate (CAS_2) phases of the ash has been considered [7]:

$$\underset{1}{2CH} + \underset{0.7538}{AS} + \underset{1.631}{6H} \rightarrow \underset{3.26}{C_2ASH_8}$$

$$\underset{1}{CAS_2} + \underset{0.886}{C_3A} + \underset{2.862}{16H} \rightarrow \underset{4.286}{2C_2ASH_8}$$

$$\underset{0.786}{CAS_2} + \underset{1}{C_4AF} + \underset{2.81}{20H} \rightarrow \underset{3.37}{2C_2ASH_8} + \underset{0.2586}{CH} + \underset{0.5453}{FH_3}$$

Finally, the presence of thenardite (Na_2SO_4) has also been detected by XRD in cement pastes containing MSWI fly ash. However, the formation of this hydrate has not been taken into account, as alkali ions are not yet represented in the CEMHYD3D model.

3. Hydration of cement in the presence of MSWI fly ash

The hydration of several cement pastes containing MSWI fly ash has been simulated. 5000 cycles of hydration have been performed for each paste (in the model, 5000 cycles represent approximately 1000 days of hydration for a pure cement paste at room temperature [5]).

3.1. Composition of the modeled cement pastes

The cement pastes P0-C1 [pure cement paste, water/cement ratio (W/C) = 0.5], P20-C1 (20% of MSWI fly ash added to the cement, W/C = 0.5), P-C1 (pure cement paste, W/C = 0.4) and P-FA (20% of MSWI fly ash as a replacement of part of the cement, W/C = 0.4) presented in the first part of the article have been modeled. Table 2 shows the volume compositions of these pastes.

Table 2
Volume compositions of the modeled cement pastes[a]

	Water (%)	Cement (%)	MSWI fly ash (%)	Dissolved chlorides (%)
P0-C1	62	38	0	0
P-C1	56	44	0	0
P20-C1	57	36	7	2
P-FA	56	37	7	2

[a] Dissolved chlorides can also be expressed as a volume fraction because, in the model, diffusing species are represented by one-pixel species diffusing within the capillary porosity.

The pastes P-C1 and P-FA have been modeled twice to assess the reproducibility of the results of the model. For the four different simulations, the initial microstructures have been completely changed. The position of the cement and MSWI fly ash particles and the phases distribution amongst the particles are thus a priori different between those pastes. The results are labeled P-C1 (1), P-C1 (2), P-FA (1) and P-FA (2).

3.2. Hydrate formation

Similar results have been obtained for the pastes P0-C1 and P-C1 (1 and 2) and for P20-C1 and P-FA (1 and 2). In the following, we only present the results obtained for one of the pastes P-C1 and P-FA. Similar observations can be made for the pastes P0-C1 and P20-C1.

Fig. 1 shows the evolution of the quantities of portlandite (CH) and C-S-H formed in the pastes P-C1 and P-FA during the 5000 cycles of hydration. These quantities are expressed as the volume of hydrate formed relative to the volume of silicates ($C_3S + C_2S$) present in the initial mix.

It can be seen in Fig. 1 that the presence of the MSWI fly ash only slightly modifies the formation of portlandite and C-S-H. The quantity of portlandite formed in the paste P-C1 is slightly higher than that formed in the paste P-FA. In the model, there are very few interactions between the constituents of the ash and the silicates of cement. Only the AS phase of the fly ash (slightly reactive) can react with dissolved portlandite to form stratlingite. So, the incorporation of fly ash in the model has little effect on the hydration of C_3S and C_2S. It only results in a slight consumption of portlandite due to the formation of stratlingite from the aluminosilicates of the fly ash.

Fig. 2 presents the volume fractions of Friedel's salt, ettringite and monosulfoaluminate formed during hydration in the two cement pastes.

Fig. 3 shows the volume fractions of the main phases of the pastes P-C1 and P-FA after 5000 cycles of hydration.

Fig. 2 shows that the kinetics of formation (and the quantities) of ettringite and monosulfoaluminate in the two cement pastes are very different. The presence of a great quantity of chlorides in the ash explains this result. In the

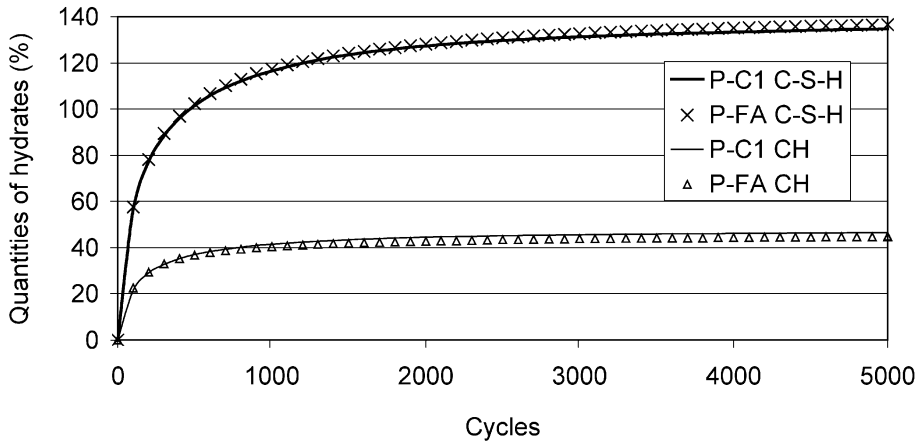

Fig. 1. Volumes of C-S-H and portlandite formed in the pastes P-C1 and P-FA reported relative to the initial volumes of silicates.

absence of chlorides (paste P-C1), there is first a very fast formation of ettringite, then ettringite dissolves and monosulfoaluminate is formed. The initial formation of ettringite corresponds to the regulation of setting of the C_3A by gypsum. At the beginning of hydration, the gypsum dissolves and forms ettringite at the surface of C_3A grains. Once gypsum has been consumed in great part by this reaction, its concentration in the interstitial solution decreases, ettringite dissolves and supplies the interstitial solution with sulfates. Monosulfoaluminate then forms and the hydration of the C_3A continues to form Afm and C_3AH_6.

The presence of chlorides in the initial mix modifies this process. From the first cycles of hydration, large quantities of chlorides (and sulfates) are present in the interstitial solution. Chlorides form Friedel's salt at the cement's aluminate surfaces (C_3A and C_4AF). In the same way, sulfates form ettringite. These two hydrates oppose one another in continuing the hydration of these grains. This explains the sudden slowing down of the formation of Friedel's salt (most of the C_3A grains have been overlaid with hydrates). There is a competition between the formation of ettringite (reaction between aluminates and sulfates) and the formation of Friedel's salt (reaction between aluminates and chlorides). So, there are less aluminates that are likely to react with sulfates than in the pure cement paste P-C1 and the sulfate concentration in the interstitial solution remains high, which slows down the dissolution of ettringite. The formation of monosulfoaluminate is therefore also slowed down. Moreover, due to the high concentrations of chlorides and sulfates, the formation of C_3AH_6 is very low. Indeed, the aluminates that are diffusing in the capillary porosity have a high probability to meet diffusing sulfates or chlorides and thus form Friedel's salt or ettringite more easily than C_3AH_6.

It has to be noted that no account was made for the influence of the sulfate concentration on the stability of Friedel's salt. Studies on the resistance of concrete to seawater [9] have shown that in the presence of sulfates, Friedel's salt dissolves to form ettringite. A high concentration of sulfates in the interstitial solution (due to the fact that C_3A reacts more easily with chlorides) could certainly lead to the redissolution of Friedel's salt and to the formation of

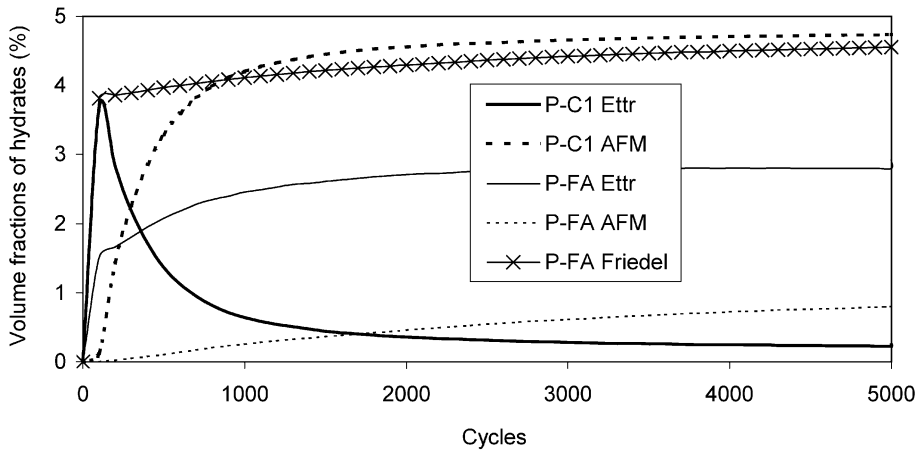

Fig. 2. Volume fractions of Friedel's salt, ettringite and monosulfoaluminate formed in the pastes P-C1 and P-FA.

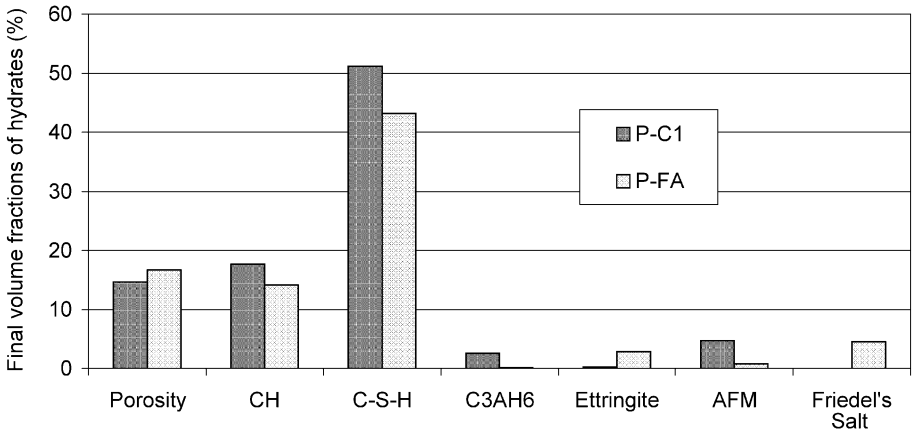

Fig. 3. Volume fractions of the main phases in the pastes P-C1 and P-FA after 5000 cycles of hydration.

ettringite. The latter could then be expansive if formed in a hardened confined material.

Kinetic aspects of the hydration have not been taken into account in the model. The interactions between the constituents of the MSWI fly ash and those of the cement are indeed very numerous and complex, and some of them are not well understood (in particular the interactions between cement and heavy metals). However, the kinetics of the reactions occurring during hydration affects the final quantities of hydrates formed. For example, the very fast formation of Friedel's salt consumes a large quantity of aluminates, which reduces the quantity of C_3AH_6 formed in the paste. So, different kinetics of hydration could modify the final microstructure of the material. However, the results of the model confirm certain experimental results obtained using XRD on cement pastes. Indeed, these tests have shown that in cement pastes containing MSWI fly ash, the quantity of Friedel's salt (after 28 days of hydration) is significant. Moreover, the quantity of ettringite formed in the presence of the MSWI fly ash is higher than that formed in pure cement pastes and the thenardite (Na_2SO_4) that has been detected in cement pastes in the presence of MSWI fly ash confirms that the concentration of sulfates in the interstitial solution of those pastes is high. Finally, workability tests performed on cement pastes containing MSWI fly ash have shown a fast decrease in the workability of these pastes with time [6]. The early and rapid formation of Friedel's salt could possibly explain this experimental result, as a rapid formation of hydration products will generally result in a significant loss of workability.

4. Modeling of leaching

4.1. Assumptions of the model

During the leaching process, the concentrations of the chemical species present in the interstitial solution decrease. The chemical equilibrium initially established is then upset. The more soluble hydrates dissolve successively in order to restore the equilibrium. Therefore, leaching results in an increase in porosity due to the dissolution of hydrates. This can in turn modify the transport properties of the material.

Vernet [10] gives the solubilities of portlandite, monosulfoaluminate, monochloroaluminate (Friedel's salt) and ettringite for different pH values. Whatever the pH, these solubilities are classified in the following order: $S_{\text{portlandite}} > S_{\text{monosulfoaluminate}} > S_{\text{Friedel's salt}} > S_{\text{ettringite}}$. During the leaching process, the phases present in cement pastes containing MSWI fly ash should dissolve in the following order: (1) portlandite, (2) monosulfoaluminate, (3) Friedel's salt, (4) ettringite and (5) decalcification of C-S-H (the latter is not taken into account in the model).

In order to describe the increase in porosity due to leaching, the dissolution of the more soluble phases of the hydrated cement paste has to be simulated. Bentz and Garboczi [11] have already modeled the leaching of portlandite in pure cement pastes. A similar algorithm has been used for cement pastes containing MSWI fly ash. This algorithm is based on the following principle:

First scan of the microstructure: each pixel of the soluble phase that is in contact with the capillary porosity is highlighted.

Second scan of the microstructure: each pixel identified in the preceding stage attempts to perform a one-pixel movement in a random direction. If the new position is occupied by a solid phase, the pixel is not dissolved. If the new position is a capillary pore, a random number between 0 and 1 is compared to a dissolution probability. If the number is lower, the pixel is dissolved (replaced by a capillary pore).

In order to assess the influence of the increase in porosity of the material on its diffusion coefficient, a random walker algorithm has been used [12,13]. This algorithm consists of dispersing random walkers in the conducting phases of the cement paste (capillary pore space and C-S-H) and computing the mean distance they travel after a large number of

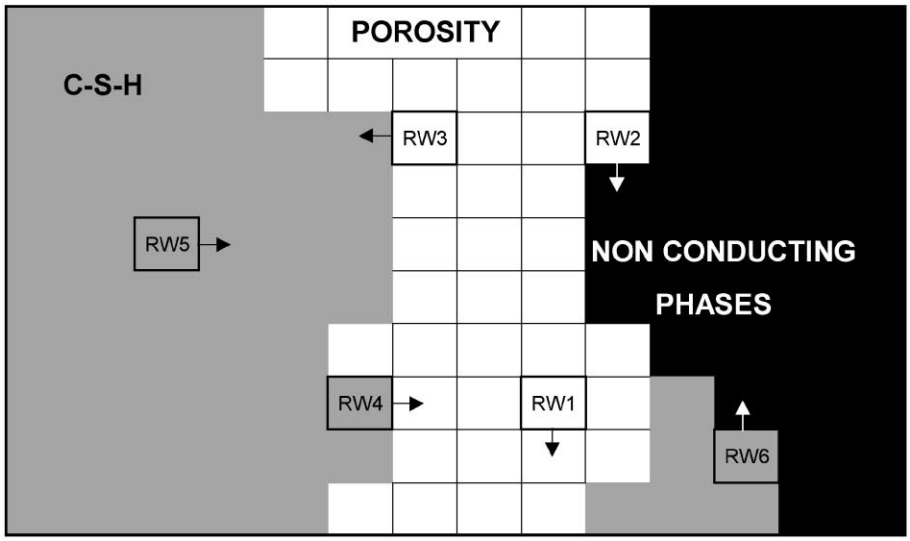

Fig. 4. Movements of the random walkers in the cement paste (the arrows indicate the random directions chosen).

time steps. The mobility of the random walkers depends on the conductivity of the phases and on their initial and final positions. The algorithm used is presented as follows.

Fig. 4 represents a hydrated cement paste in two dimensions in which six random walkers have been dispersed (RW1, RW2, RW3, RW4, RW5 and RW6). Each of those random walkers can perform a random walk (left, right, up or down). This example is in two dimensions. In our simulations, cement pastes are in three dimensions and random walkers can perform six different walks each time step. The moving conditions for going from the initial to the final position are presented in Table 3. The mobility of the random walkers in a particular phase is represented by a probability for the random walker to go from the initial to the final position. When a random direction has been chosen, a random number between 0 and 1 is compared to that probability. If it is lower, the walk is performed; otherwise, the random walker remains at its original position.

The probability for a random walker to step from one position to another in a given phase depends on the conductivity of that phase. Supposing that two adjacent pixels are linked by a conductor, the conductance of that link can be calculated as follows [14]:

$$\Sigma_{ij} = \frac{1}{\frac{1}{\Sigma_i} + \frac{1}{\Sigma j}} \quad (1)$$

where Σ_i is the conductance of half a pixel ($\Sigma_i = \sigma_i d^2/(0.5d) = 2d\sigma_i$, σ_i being the conductivity of the phase and d the length of one pixel).

Chloride ion diffusion in the C-S-H gel of a pure cement paste is about 400 times smaller than in the capillary pore space [14–16]. The ratio of the conductivities of these two phases can therefore be estimated to about 1/400 [14], although rigorously, the conductivity depends on the type of ion considered (this ratio could be different for chemical species other than chloride). We assumed that the ratio of the conductivities of chemical species in the C-S-H and in the capillary pore space, in cement pastes containing MSWI fly ash, is also 1/400. Indeed, DSC tests performed on cement pastes containing MSWI fly ash (first part of the article [4]) have shown that the structure of the C-S-H in those pastes is similar to that of C-S-H formed in pure cement pastes.

The probability of moving for the random walkers equals the equivalent conductance Σ_{ij} calculated by Eq. (1), with $d = 1$, $\sigma_{\text{porosity}} = 1$ and $\sigma_{\text{C-S-H}} = 1/400$.

The probability for a pixel to move from a C-S-H ($\sigma_i = 1/400$) to a capillary pore ($\sigma_j = 1$) is therefore given by:

$$p = \frac{1}{\frac{1}{2\frac{1}{400}} + \frac{1}{2}} = \frac{1}{200.5}.$$

The mean value of the squared distance covered by the random walkers is then calculated ($<R^2>$). For a large number of time steps, the function $<R^2> = f(t)$ tends to a straight line whose slope equals the ratio between the diffusion coefficients in the porous phases (C-S-H + capillary pore space) and the diffusion coefficient in the interstitial solution. By multiplying this ratio by the volume

Table 3
Moving conditions for the random walkers to go from one phase to another

	Initial position	New position	Movement probability
RW1	Porosity	Porosity	1
RW2	Porosity	Nonconducting phase	0
RW3	Porosity	C-S-H	1/200.5
RW4	C-S-H	Porosity	1/200.5
RW5	C-S-H	C-S-H	1/400
RW6	C-S-H	Nonconducting phase	0

fraction V_{por} of the porous phases, the effective diffusivity of the cement paste is obtained (Eq. (2)).

$$\frac{D}{D_0} = \frac{< R^2 >}{t} V_{por} \quad (2)$$

All of our simulations have been performed with 5000 random walkers and 2×10^6 time steps.

4.2. Results and discussion

The hydrated pastes P0-C1, P20-C1, P-C1 (1 and 2) and P-FA (1 and 2) have been leached using the algorithm presented above. Given the large quantities of portlandite present in those pastes, the increase in porosity during leaching results mainly from the dissolution of this phase.

4.2.1. Connected capillary porosity

The evolution of the connected capillary porosity of the pastes during leaching has first been studied. Connected capillary porosity significantly affects the transport properties of the material. It has been determined by counting the pixels of capillary porosity contained in continuous pathways crossing the microstructure. When the capillary pore space is not percolated (that is to say when there is no continuous pathway crossing the microstructure), the connected fraction of capillary porosity equals zero.

Fig. 5 shows the connected fraction of capillary porosity as a function of total capillary porosity for each cement paste. The results given in Fig. 5 have been obtained by taking the mean value of the connected fraction of capillary porosity in the three principal directions *X*, *Y* and *Z*.

The curves obtained generally present three different zones: For the low values of capillary porosity, the percolation threshold of the capillary pore space has not been reached and there is no continuous pathway of capillary porosity, the connected fraction therefore equals zero.

As the percolation threshold is reached, the connected fraction of capillary porosity increases abruptly.

For higher values of capillary porosity, the connected fraction approaches 100% and increases more slowly.

The curves obtained for the pastes P0-C1, P20-C1, P-FA (1) and P-FA (2) are very similar. The initial porosity of the paste P0-C1 (24.3%) is high and the first part of the curve cannot be seen because the capillary pore space is already percolated, with a connected fraction of about 68%. For the paste P20-C1, the capillary porosity after 5000 cycles of hydration (18.8%) is very close to the percolation threshold. Indeed, the capillary pore space was percolated in the *X* direction but not in the two other directions.

The capillary porosity of the pastes P-FA (1) (16.7%) and P-FA (2) (17.0%) after 5000 cycles of hydration are beyond their percolation threshold (about 19%). Their connected fraction is therefore zero until the percolation threshold is reached.

The curves obtained for the pure cement pastes P-C1 (1) and P-C1 (2) are quite different from the other pastes. Their capillary porosities after 5000 cycles of hydration are 15.1% and 14.7%, respectively. The percolation threshold of those pastes (about 17.5%) is lower than that of pastes P-FA (1 and 2). The curves of pastes P-C1 (1 and 2) are above the curves of pastes P-FA (1 and 2), that is to say for a given capillary porosity, the connected fraction is higher.

The incorporation of MSWI fly ash as a replacement of part of the cement in the pastes P-FA (1 and 2) explains the higher porosity of those pastes with regard to pastes P-C1 (1 and 2). Indeed, MSWI fly ash particles are far less reactive than the cement grains they are replacing. The quantities of hydrates formed (C-S-H and portlandite in particular) in the P-FA pastes are thus smaller than in the P-C1 pastes (see Fig. 3). The capillary porosity of the latter is therefore lower.

The difference in percolation threshold between the systems with and without fly ash is most likely due to their difference in volume fraction of nonleachable phases (C-S-H and C_3AH_6). Since the system without fly ash contains more of these nonleachable phases (Fig. 3), the leaching process within this paste will in effect be more efficient, based on the

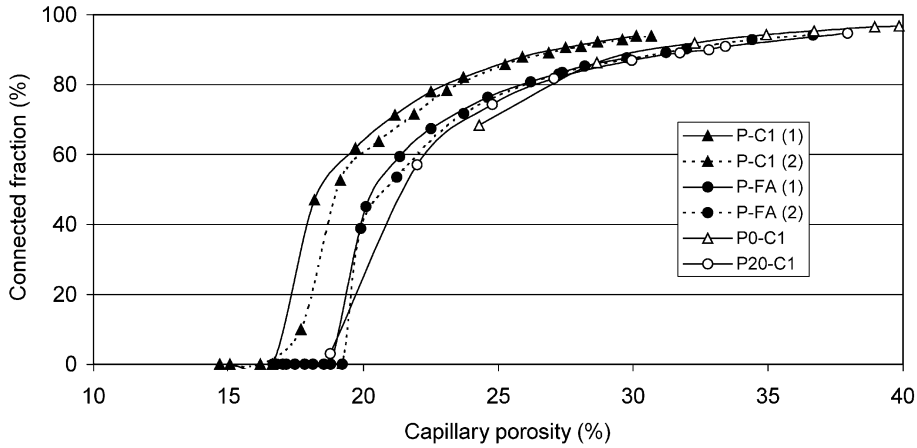

Fig. 5. Connected fraction of capillary porosity as a function of total capillary porosity of the pastes during leaching.

assumption that "pore" products such as CH are more important in depercolating the pore space between particles than "surface" products such as C-S-H [11]. In the system with fly ash, some of these C-S-H pixels have been replaced by leachable phases such as Friedel's salt, but such pixels may do little to percolate the capillary porosity when they are leached away.

4.2.2. Diffusivity

Fig. 6 presents the evolution of the effective diffusivity of the pastes P0-C1, P20-C1, P-C1 (1 and 2) and P-FA (1 and 2) during leaching (determined using the random walkers algorithm presented above). The curve obtained by Garboczi and Bentz [14] for *pure C_3S pastes during hydration* is indicated by the solid line. The equation of this curve is:

$$D/D_0 = 0.001 + 0.07\Phi^2 + H(\Phi - \Phi_c)1.8(\Phi - \Phi_c)^2 \quad (3)$$

with $H(x)$ = Heaviside function; Φ = capillary porosity; Φ_c = capillary porosity percolation threshold, 0.18 and D_0 = diffusion coefficient in the interstitial solution.

Previous leaching simulations [11] have indicated that the diffusivities obtained after leaching lie significantly above the curve given by Eq. (3). However, these results [11] were obtained for systems based on pure C_3S. In the current study, all of the hydration reactions for a Portland cement (and fly ash) have been utilized. For *Portland cements*, the diffusivity curve obtained during hydration has been found to lie below Eq. (3) [17]. Leaching will again "raise" this curve so that in the end, as can be seen in Fig. 6. Eq. (3) gives a satisfactory but not perfect description of the leaching results we have obtained. For a given capillary porosity, the effective diffusivity of P-FA pastes is slightly lower than that of P-C1 pastes. This confirms the observations made above concerning the connected fraction of the capillary porosity. During leaching, the effective diffusivity of cement pastes can increase significantly. For example, the effective diffusivity D/D_0 of the paste P-FA (1) after hydration is 1.8×10^{-3} (capillary porosity = 16.7%). This diffusivity increases by a factor of nearly 20 up to 34.5×10^{-3} (capillary porosity = 29.8%) after leaching 91% of the portlandite initially present in the paste.

5. Taking into account the evolution of the microstructure in a simplified leaching model

The increase in porosity due to the dissolution of hydrates during leaching leads to an increase in the diffusion coefficient of the material. To assess the importance of the modification of the diffusion coefficient on the kinetics of leaching, the relation $D = f(\Phi)$ determined in the last paragraph has been incorporated into a simplified leaching model. The objective of this model is to assess the influence of the evolution of the microstructure on the leaching process. The aim of the model is not to give a realistic simulation of the dissolution of the different hydrates in cement pastes containing MSWI fly ash. The chemical equilibria involved in this material are very complex and were not assessed precisely in this study.

A simplified leaching model, taking into account one soluble phase (portlandite) and two chemical species in solution (calcium and sodium), has been developed. This model allows one to simulate the increase in porosity due to the dissolution of the soluble phase during leaching and to study the influence of this increase on the kinetics of the release of chemicals into the environment.

5.1. Assumptions and equations of the model

In order to simplify the calculations, leaching has been simulated in one direction. The leached sample is a bar of fixed cross-section (S), 10 mm long, completely immersed in a leaching solution. We assume that leaching occurs only from the two ends of the bar, the sides of the bar being

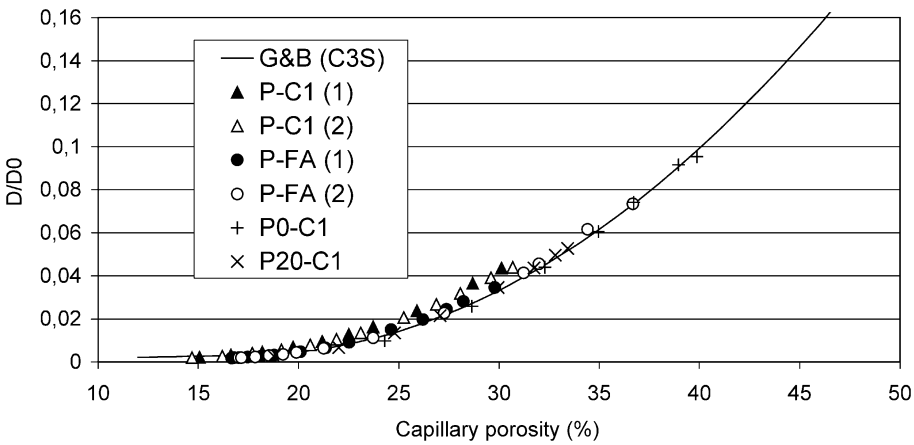

Fig. 6. Evolution of the effective diffusivity of the pastes P0-C1, P20-C1, P-C1 (1 and 2) and P-FA (1 and 2) during leaching. The curve corresponding to Eq. (3), obtained by Garboczi and Bentz [14], is also presented.

sealed. The symmetry of the problem allows one to solve the equations only in half of the bar.

The following assumptions were made:

- The bar is continuously saturated.
- Transport of chemical species occurs only by diffusion.
- The diffusion coefficients of the chemical species within the interstitial solution are constant (in particular, they do not depend on the concentrations) and they are identical for all the chemical species studied.

Two chemical species were taken into account: calcium and sodium. During leaching, the dissolution of portlandite supplies the solution with calcium. However, sodium is only present in the solution. The transport equations for these two species are (Eqs. (4) and (5)):

$$\frac{\partial C_{Na}}{\partial t} = \frac{\partial}{\partial x}\left(D_{app}\frac{\partial C_{Na}}{\partial x}\right) \qquad \text{for sodium} \tag{4}$$

$$\frac{\partial C_{Ca}}{\partial t} = \frac{\partial}{\partial x}\left(D_{app}\frac{\partial C_{Ca}}{\partial x}\right) - \frac{\partial S}{\partial t} \qquad \text{for calcium} \tag{5}$$

with C_{Na} = sodium concentration in solution (kg/m^3 of solution), C_{Ca} = calcium concentration in solution (kg/m^3 of solution), S = portlandite concentration in the material (kg/m^3 of porous material) and D_{app} = apparent diffusion coefficient of the chemical species in solution (m^2/s).

We assume that the kinetics of dissolution of portlandite is very high with regard to the kinetics of diffusion (local equilibrium assumption). In the model, as long as portlandite is present, the concentration of calcium in solution (which decreases because of leaching) is permanently maintained at the saturation concentration of portlandite. The equation determined in the last paragraph (Eq. (3)) linking capillary porosity and effective diffusivity of cement pastes containing MSWI fly ash is used in order to determine the evolution of the effective diffusion coefficient of the chemical species in solution.

The apparent diffusion coefficient D_{app} used in the transport equations is determined by dividing the effective diffusion coefficient calculated above by the total porosity Φ_{tot} of the material. This total porosity is the sum of the capillary porosity and the porosity of the C-S-H. In our simulations, we have considered that the volume fraction of the C-S-H in the material was 45% (see Fig. 3) and that the porosity of the C-S-H gel is 28% [18].

We have decided to solve the diffusion problem by using the finite difference method (explicit method) [19]. The bar is divided into N cells of length Δx. The cell $i = 0$ represents the environment (leaching solution), while the cell $i = N$ represents the center of the material. In each cell, the chemical composition of the interstitial solution, the mineralogical composition of the solid phases and the properties of the material are assumed to be uniform.

In the explicit method, all values of Δt are not suitable for the calculation of concentrations. The stability condition for an internal node is [20]:

$$\frac{\Delta x^2}{D\Delta t} \geq 2q \tag{6}$$

where q is the number of geometrical variables in the problem (in our case, $q = 1$). As the diffusion coefficient in the damaged zone increases, Eq. (6) has to be respected for all the possible values of the diffusion coefficient. In the simulations presented here, this criterion was respected by a factor of 2.3 in the damaged zone and 21.9 in the undamaged zone.

5.1.1. Boundary conditions

The leaching solution is demineralized water that is frequently renewed, so it is assumed that the calcium and sodium concentrations are permanently zero.

Given the symmetry of the problem (unidirectional leaching of a bar from its two ends), the concentration in the last cell ($i = N$) is equal to the concentration of the fictive cell ($i = N + 1$).

5.1.2. Initial conditions

It is assumed that at the beginning of leaching, the interstitial solution of the material is saturated with respect to portlandite and that the sodium concentration in the bar is uniform.

5.2. Results and discussion

Figs. 7 and 8 present, respectively, the release of calcium and sodium as a function of the square root of time during leaching, taking into account the evolution of the diffusion coefficient of the material. Curves corresponding to the release of those chemical species with a constant diffusion coefficient (equal to the diffusion coefficient of the undamaged material) are also presented.

The release of calcium is more important when the evolution of the diffusion coefficient is taken into account (Fig. 7). This release is proportional to the square root of time for the two calculations. So, a constant fictitious diffusion coefficient, higher than the initial diffusion coefficient of the material, can be found that would lead to an identical release of calcium as that obtained by taking into account the evolution of the diffusion coefficient.

Fig. 8 shows that the release of sodium is at first proportional to the square root of time and then decreases. This decrease corresponds to the depletion of sodium inside the material. Unlike calcium, taking into account the evolution of the diffusion coefficient does not modify the release of sodium for the following reason. The decrease in release due to the depletion of sodium occurs about after 50 h. At that time, only five cells have been damaged (that is to say that in those cells, portlandite has been completely dissolved). Unlike calcium, sodium is not supplied into solution by the dissolution of a solid phase. Therefore, the transport equation for sodium (Eq. (4)) does not contain a source term. The

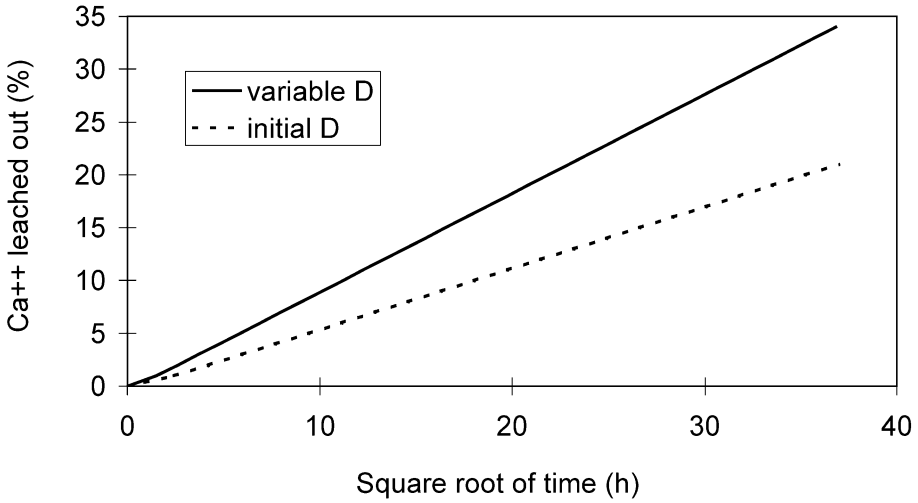

Fig. 7. Quantity of calcium leached out as a function of square root of time.

changes in the diffusion coefficient thus affect only a very small zone of the material (5%). The diffusion of sodium then leads to the depletion of that chemical species long before the dissolution of portlandite can significantly alter the transport properties of the material.

These results first show that for each chemical species studied (calcium and sodium), a constant diffusion coefficient can be used to describe the release observed by taking into account the evolution of the microstructure. The initial diffusion coefficient of the material allows one to describe the release of sodium. The evolution of the transport properties of the material does not affect the release of that element. Indeed, sodium is not renewed into solution during leaching. Its release is very fast (compared to the dissolution of portlandite) and occurs before the degradation due to leaching affects a significant depth of the material. So, *the diffusion coefficient determined from the release of sodium during a leaching test may not take into account the aging of the material*.

The release of calcium can also be described with a constant diffusion coefficient (in our simulations, $D_{cst} = 9.96 \times 10^{-3} D_0$). This diffusion coefficient is higher than the diffusion coefficient of the undamaged zone of the material (initial diffusion coefficient $= 3.57 \times 10^{-3} D_0$) but lower than that of the totally damaged zone (final diffusion coefficient $= 4.92 \times 10^{-2} D_0$). A constant diffusion coefficient allows one to describe the release of calcium at any time. Although this coefficient does not take into account the evolution of the microstructure throughout time, it does not underestimate the long-term transport properties of the material. It could be used, for example, to simulate the long-term release of calcium in cement pastes containing MSWI fly ash and allow one to determine the pH profile (linked to the presence of portlandite) in the interstitial solution of the material. Although the release of calcium can be simulated with a constant diffusion coefficient, the transport properties of the material are not homogeneous during leaching. In particular, the diffusion coefficient in the damaged zone, in

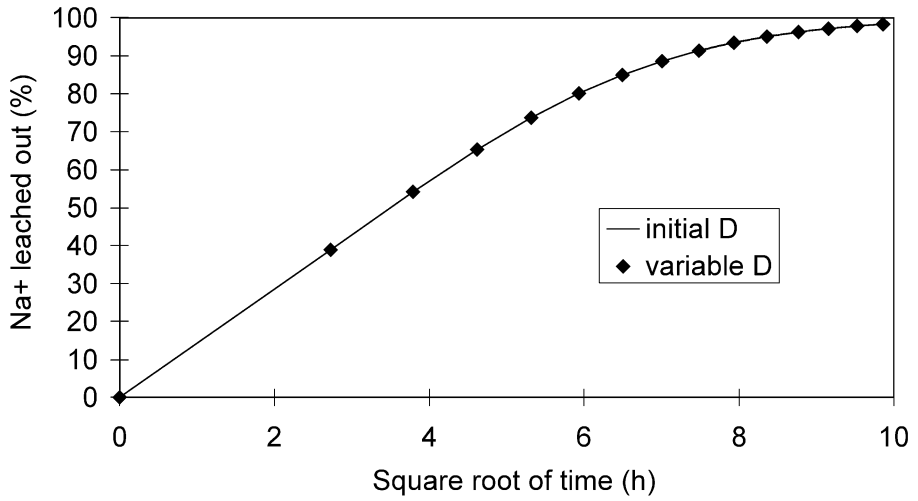

Fig. 8. Quantity of sodium leached out as a function of square root of time.

contact with the leaching solution, is maximal. This modification of the surface transport properties of the material could have a significant influence on durability. Indeed, the increase in diffusivity and in permeability in this zone would allow an easier ingress of water and aggressive agents inside the material. In this way, the kinetics of penetration of aggressive agents into the material could be more affected by the evolution of the microstructure than the kinetics of release. In fact, the aggressive agents would enter the material via the damaged zone. In a similar way, a decrease in surface porosity, in particular due to carbonation, could significantly affect the durability of the material.

6. Conclusions

The experimental study carried out has characterized the MSWI fly ash [4] in order to incorporate it into the hydration model developed at NIST by Bentz and Garboczi and to take into account its interactions with the constituents of cement. The results of the model show that the MSWI fly ash essentially affects the hydration of the aluminate phases of the cement, in particular by forming Friedel's salt. The reactions between chlorides and aluminates lead in particular to a high sulfate concentration in the interstitial solution of cement pastes. This slows down the transformation of ettringite into monosulfoaluminate. These results confirm certain experimental observations carried out on cement pastes containing MSWI fly ash: the presence of large quantities of ettringite and Friedel's salt and the presence of thenardite indicating a high sulfate concentration in the interstitial solution.

The model has also been applied to studying the evolution of the microstructure of cement pastes containing MSWI fly ash during the leaching process. The increase in the diffusion coefficient of these pastes as a function of the increase in capillary porosity due to the dissolution of hydrates has in particular been studied. This study has shown that the diffusion coefficient of cement pastes containing MSWI fly ash evolves in a similar way as pure cement pastes during leaching (for fly ash contents lower than 20%). Moreover, although the replacement of part of the cement by MSWI fly ash leads to an increase in capillary porosity of hydrated cement pastes, the percolation threshold of the capillary pore space of those leached pastes is higher than that of pure leached cement pastes. In the same way, the connected fraction of capillary porosity, for a given value of the capillary porosity, is lower in the cement pastes containing MSWI fly ash than in pure cement pastes. This increase in percolation threshold may be due to the increased concentration of capillary porosity around the large fly ash particles.

Finally, a simplified macroscopic leaching model has been developed in order to assess the influence of the increase in diffusion coefficient on the kinetics of leaching. This model simulates the release of calcium (renewed into solution by the dissolution of portlandite) and the release of a free chemical species into solution (sodium) that is not renewed by the dissolution of a solid phase. The model shows that the release of chemical species like sodium is not affected by the modifications of the transport properties. Indeed, the release of such species is, in general, very fast in comparison to the kinetics of degradation of the material. However, the increase in the diffusion coefficient in the damaged zone leads to an increase in the release of calcium. This release can be simulated with a constant diffusion coefficient, with a value higher than that of the initial diffusion coefficient but lower than that of the totally damaged (leached) zone.

The macroscopic leaching model showed that modifications of the microstructure can affect the kinetics of release of chemical species that are associated with a solid soluble phase. However, this simplified macroscopic model does not take into account several solid phases. Taking into account the relation between the diffusion coefficient and the capillary porosity, in a leaching model considering several solid phases, would allow one to assess the influence of the modification of the microstructure on the release of pollutants. This influence would certainly be limited for pollutants whose release depends on a chemical context. In addition, the kinetics of the release of portlandite affects the pH profile in the material in a significant way. It thus also affects the dissolution of the phases whose solubility depends on pH (such as amphoterous metals).

The leaching process, as it has been simulated in our study, assumes that the material is constantly saturated with respect to water and that there is no carbonation. In real conditions, in particular for construction materials, concrete is very often not saturated and is subjected to carbonation. The latter leads in particular to a decrease in surface porosity of the concrete. Carbonation would also certainly affect in a large way the ingress of exterior agents into the concrete (water, aggressive chemical species, etc.) and the release of chemical species into the interstitial solution. The hydration model used in this study to simulate the increase in porosity due to the dissolution of hydrates could also be used to study the decrease in porosity due to carbonation. This would allow one to take into account carbonation in the simulation of leaching and to better approach the real in-use conditions of concrete construction.

Acknowledgments

One of the authors (S. Rémond) would like to thank ADEME for their financial support. The authors also thank Vicat for executing the chemical and size grading analyses of the MSWI fly ash and Cylergie for interpreting the fly ash and cement paste XRD diagrams. The assistance of Paul Stutzman (BFRL/NIST) in performing the SEM analysis is greatly appreciated. S. Rémond would also like to

thank the staff of BFRL for their hospitality during his 6-month stay at NIST.

References

[1] S. Rémond, Evolution de la microstructure des bétons contenant des déchets au cours de la lixiviation, PhD thesis at l'Ecole Normale Supérieure de Cachan defended November 17, 1998.
[2] S. Rémond, P. Pimienta, P. Kalifa, Incorporating waste into the preparation of concrete: Bases for an assessment methodology, Second International Conference Building and the Environment, Paris, June 9–12, CSTB, Paris, 1997, pp. 659–668.
[3] D.P. Bentz, E.J. Garboczi, A digitized simulation model for microstructural development, Adv. Cem. Mater., Ceram. Trans. 16 (1991) 211–226.
[4] S. Rémond, P. Pimienta, D.P. Bentz, Effects of the incorporation of Municipal Solid Waste Incineration fly ash in cement pastes and mortars: I. Experimental study, Cem. Concr. Res., 2002 (in press).
[5] D.P. Bentz, Three-dimensional computer simulation of Portland cement hydration and microstructure development, J. Am. Ceram. Soc. 80 (1997) 3–21.
[6] S. Rémond, P. Pimienta, N. Rodrigues, J.P. Bournazel, Assessing the properties of mortars containing Municipal Solid Waste Incineration fly ash, in: R.W. Dhir., M.J. McCarthy (Eds.), International Congress Creating with Concrete, University of Dundee, September 6–10, 1999, pp. 319–326.
[7] D.P. Bentz, S. Rémond, Incorporation of Fly Ash into a 3-D Cement Hydration Microstructure Model, NISTIR 6050, U.S. Department of Commerce, 1997, NIST, Gaithersburg, February (available at http://ciks.cbt.nist.gov/bentz/flyash/flyash.html.).
[8] B. Kessler, M. Rollet, F. Sorrentino, Microstructure of cement pastes as incinerator ash host, in: R.W. Piggot (Ed.), Proceedings of the First International Symposium on Cement Industry Solution to Waste Management, Calgary, 1992, pp. 235–251.
[9] M. Regourd, L'action de l'eau de mer sur les ciments, Ann. Inst. Tech. Batim. Trav. Publics 329, 1975, 86–102.
[10] C. Vernet, Stabilité chimique des hydrates — Mécanismes de défense du béton face aux agressions chimiques, in: La durabilité des bétons, sous la direction de J. Baron et J.P. Ollivier, Presses de l'Ecole Nationale des Ponts et Chaussées, 1992, pp. 129–169.
[11] D.P. Bentz, E.J. Garboczi, Modelling the leaching of calcium hydroxide from cement paste: Effects on pore space percolation and diffusivity, Mater. Struct. 25 (1992) 523–533.
[12] E.J. Garboczi, L.M. Schwartz, D.P. Bentz, Modeling the influence of the interfacial zone on the DC electrical conductivity of mortar, Adv. Cem. Based Mater. 2 (1995) 169–181.
[13] D.C. Hong, H.E. Stanley, A. Coniglio, A. Bunde, Random-walk approach to the two-component random-conductor mixture: Perturbing away from the perfect random resistor-network and random superconducting-network limits, Phys. Rev. B 33 (7) (1986) 4564–4573.
[14] E.J. Garboczi, D.P. Bentz, Computer simulation of the diffusivity of cement-based materials, J. Mater. Sci. 27 (1992) 2083–2092.
[15] A. Atkinson, A.K. Nickerson, J. Mater. Sci. 19 (1984) 3068–3078.
[16] C.L. Page, N.R. Short, A. El Tarras, Cem. Concr. Res. 11 (1981) 395–406.
[17] D.P. Bentz, O.M. Jensen, A.M. Coats, F.P. Glasser, Influence of silica fume on diffusivity in cement-based materials: I. Experimental and computer modeling studies on cement pastes, Cem. Concr. Res. 30 (2000) 953–962.
[18] T.C. Powers, T.L. Brownyard, Studies of the physical properties of hardened Portland cement paste, ACI J. Proc. 43 (1–9) (1946) 47–48.
[19] J. Crank, The Mathematics of Diffusion, second ed., Clarendon Press, Oxford, 1975.
[20] F. Kreith, Transmission de la chaleur et thermodynamique, Masson, Paris, 1976.